

A Study on 3D Printed CFRP-Metal Sandwich Structures for Hydrogen Transportation and Storage in Aerospace and Automotive Systems

Mebin Varghese¹, Arivazhagan Anbalagan^{1,2*}, Shone George², Marcos Kauffman²

¹Faculty of Computing and Engineering, Priory Street, Coventry University, Coventry CV1 5FB, United Kingdom.

²The Institute for Advanced Manufacturing & Engineering, (AME), Beresford Avenue, Coventry University, CV6 5LZ, United Kingdom

Abstract. This study investigates the mechanical performance of 3D-printed Carbon Fiber Reinforced Polymer (CFRP)-metal sandwich structures, focusing on infill pattern, infill ratio, and build orientation. The work primarily targets lightweight applications in hydrogen storage for aerospace and automotive sectors. Tensile and flexural tests were first conducted on non-sandwich specimens based on an earlier study [1], considering (i) infill patterns - Gyroid and Triangular and (ii) infill ratios - 30%, 40%, and 52%. In tensile tests, strength increased with infill ratio, with Triangular infill consistently outperforming Gyroid, peaking at 863 N (Triangular 52%) versus 777.5 N (Gyroid 52%). Lower displacement in Triangular indicated higher stiffness. Flexural tests on non-sandwich specimens showed Gyroid 40% achieving the highest load (644.85 N), while Triangular 52% exhibited steady strength gains with increasing density. Selected configurations were further tested in sandwich structures (CFRP–stainless steel with nickel coating), where Gyroid 40% demonstrated the highest load-bearing capacity (1008.55 N), followed by Triangular 52% (717.09 N). Notably, Gyroid 52% showed the greatest extension (14.38 mm) despite lower strength, indicating enhanced ductility. Overall, the results highlight a trade-off between stiffness and compliance, suggesting Triangular infill for high-strength, rigid components and Gyroid for balanced flexural performance. Overall, this work provides an impactful study on optimizing CFRP-metal hybrid designs for hydrogen storage systems.

1 Introduction & Literature Review

As we strive toward achieving carbon net-zero targets, the role of Hydrogen (H₂) as a clean energy fuel has become increasingly vital, especially in its application for transportation and day-to-day energy needs. Despite its promise, practical implementation remains limited due to challenges [2] associated with hydrogen's low volumetric density (H₂ gas @ Standard Temperature and Pressure (STP), $\rho \approx 0.0899$ kg/m³) and the high pressures required for

* Corresponding author: ad8181@coventry.ac.uk

storage (e.g., 700 bar to store 1 kg in ~16 litres). In contrast, gasoline has a much higher volumetric density ($\rho \approx 740 \text{ kg/m}^3$), stored at ambient pressure with 1 kg occupying only ~1.35 litres. Furthermore, hydrogen offers a significantly higher gravimetric energy density (~33.6 kWh/kg) compared to gasoline (~12.0 kWh/kg), making it a lightweight yet energy-rich fuel. Additionally, hydrogen combustion produces zero CO₂ emissions, whereas burning 1 kg of gasoline emits approximately 3.1 kg of CO₂, highlighting hydrogen’s potential for decarbonizing energy systems. To address these challenges, international standards such as ISO 11119 and SAE J2579 [3,4] define design and safety requirements for high-pressure vessels used in hydrogen systems. Researchers have long explored various storage methods, and five primary vessel types (Type I- V) have emerged [5]. Fig. 1(a) presents the in-house developed CAD model of a hydrogen storage tank, created as a representative design for simulation and further structural analysis. To enhance practical relevance, an image of a real CFRP hydrogen storage tank (Fig 1(b)) available in our laboratory has also been included for comparison. Fig. 1(c) compares the gravimetric density of four hydrogen vessel types normalized by wall thickness. Type I vessels are all-metal, typically carbon steel or aluminium alloys, handling pressures up to 20 MPa / 200 bars. Type II adds hoop-wrapped composites for moderate weight savings and pressures up to 25-30 MPa / 250-300bars. Type III uses full composite wraps over metal liners for pressures up to 70 MPa / 700 bars, while Type IV employs polymer liners with carbon-fibre overwraps for ultra-lightweight performance at similar pressures. Type V, still under development, is linerless and fully composite, promising maximum weight reduction and ultra-high-pressure capability [5,6]. These classifications, governed by ISO and SAE standards [3,4], ensure structural integrity and safety in automotive and aerospace hydrogen applications.

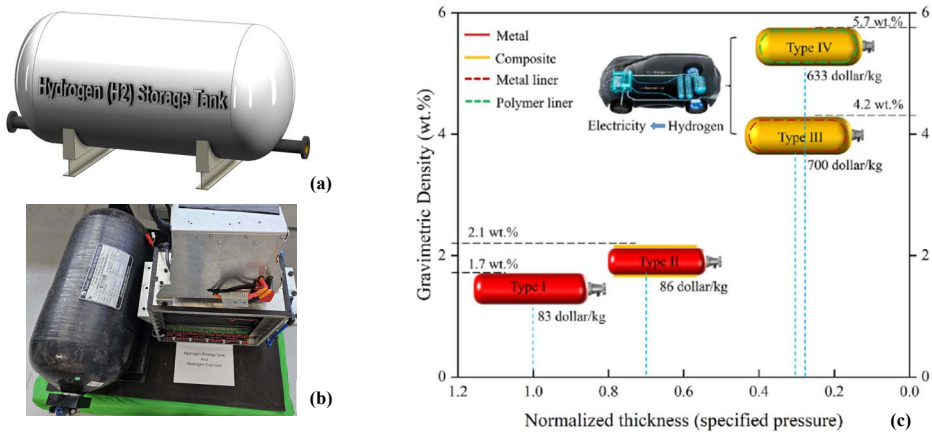


Fig. 1. (a) CAD model of a hydrogen storage tank (b) real CFRP hydrogen storage tank (c) Gravimetric density of four vessel types normalized by wall thickness [5]

In this context, the current research addresses a critical aspect of hydrogen infrastructure: the mechanical and structural stability of composite sandwich structures that could complement these vessel systems. Specifically, we investigate CFRP combined with metal layers, utilising 3D printing to fabricate lightweight yet robust components. These hybrids are promising for hydrogen containment due to their high strength-to-weight ratio and resistance to environmental degradation. This study systematically explores these factors building upon an earlier work [1] to understand their influence on bonding quality, tensile and flexural strength, and overall integrity by studying build parameters such as layer thickness, infill density, and orientation. By validating CFRP-metal sandwiches, the project supports safer,

more efficient hydrogen storage solutions aligned with ISO and SAE guidelines [3,4], contributing to clean energy technologies in automotive, aerospace, and energy sectors.

2 Literature Review

This review explores recent advancements in CFRP-based hydrogen storage technologies, focusing on bonding strategies, material optimization, and additive manufacturing approaches to enhance structural integrity and performance. Eun J.H. et al. [6] explored liner materials for Type IV hydrogen storage vessels, comparing high-density polyethylene (HDPE) with low-molecular-weight polyamide 6 (PA6). MMPA6 liners demonstrated superior mechanical strength and hydrogen barrier performance due to chemical bonding with carbon fibre-reinforced polymer (CFRP) epoxy. Katsumata et al. [7] proposed a dome cylinder split-moulded CFRP hydrogen tank structure aimed at reducing carbon fibre usage. Finite element analysis and burst testing revealed cohesive failure, while stress optimization improved joint performance. Ubaid et al. [8] investigated the influence of graphene nanoplatelets (GNPs) on CFRP composites under cryogenic thermal cycling, showing improved strength and reduced microcracking. Qi et al. [9] examined nanosecond pulsed laser treatment to enhance interfacial bonding between polyamide 11 (PA11) liners and CFRP, with optimal parameters improving peel and tensile strength. Zhou et al. [10] studied impact resistance of CFRP laminates with mismatch angles (24° – 60°), finding smaller angles improved damage tolerance and energy dissipation. Wang et al. [11] proposed a micromechanics-based fatigue life prediction method for CFRP hydrogen vessels under cyclic loading, with MATLAB simulations validating long-term durability. Graziosi et al. [12] introduced a three-dimensional (3D) printed beam-based structure to improve adhesion in metal-composite joints via mechanical interlocking. Liu et al. [13] reviewed additive manufacturing of continuous fibre-reinforced polymer (CFRP) composites, identifying opportunities in trajectory planning and multifunctional integration. Wu et al. [14] investigated sandblasting and activation pretreatment for electroless nickel adhesion to CFRP, achieving a 131% increase in adhesion strength.

Pizzorni [15] focused on adhesive bonding in 3D-printed short and continuous carbon fibre composites, emphasizing joint geometry and adhesive selection for reliable interfaces. The study by Lestari et al. [16] focuses on optimizing 3D printing parameters for CFRP using the Taguchi method. The work evaluates the effects of nozzle temperature, infill density, layer thickness, orientation, and other factors on hardness and impact strength. Findings highlight layer thickness and infill density as dominant contributors to mechanical performance, offering guidelines for improved CFRP additive manufacturing. Abualbandora et al. [17] present a comprehensive review of 3D printing short CFRP, focusing on how process parameters such as layer height, infill density, orientation, and temperature affect mechanical and thermal performance. The paper also discusses failure mechanisms, optimization strategies, and future directions for improving strength and sustainability in additive manufacturing. Yan et al. [18] proposed a stepwise parameter planning methodology for 3D printing CFRP composites using prepreg–resin co-extrusion. The study optimizes relative extrusion coefficient, layer thickness, and hatch spacing to achieve high flexural strength (243 MPa) and interlaminar shear strength (25.6 MPa), offering a systematic framework for improving composite performance. Bendine et al. (2022) [19] experimentally and numerically characterized 3D-printed continuous CFRP using FDM, focusing on tensile, interlaminar shear, fatigue, and thermal behavior. The study reports promising tensile strength (up to 738 MPa) and stiffness but highlights challenges such as void content and limited fiber volume fraction, suggesting optimization for improved performance.

Collectively, these studies advance bonding strategies, fiber placement optimization, and predictive modelling critical for designing CFRP-metal sandwich structures with superior mechanical performance in aerospace and automotive applications.

3 Methodology

This study involves 3D printing of CFRP and testing CFRP-metal sandwich structures. Key build parameters such as infill ratio, infill pattern, and layer configurations are selected based on material properties and insights from our previous study (Anbalagan et al., [1]). In the earlier work, we systematically evaluated infill ratio and pattern effects on CFRP parts using Onyx material and a Markforged Mark 2 printer. Triangular infill at 85% ratio demonstrated superior tensile performance (≈ 5.6 mm extension at ≈ 700 N), while gyroid infill at 37% ratio provided the highest flexural strength (≈ 5.6 mm at ≈ 350 N). Other patterns such as rectangular, hexagonal, and solid were de-prioritized due to lower load-extension responses. Printing parameters included a 0.125 mm layer height, nozzle temperature of 270 °C, and system-defined perimeters. These findings guided the current work in selecting optimal patterns for mechanical performance and sustainability. Tensile tests are conducted on CFRP specimens, while flexural tests assess the bending behaviour and structural integrity of both CFRP and CFRP-metal sandwiches. This systematic approach ensures a comprehensive evaluation of mechanical performance and structural reliability.

3.1 Materials, Equipment & Standards

3.1.1 Tensile & Flexural Testing Standard

Table 1. Standard Specimen Dimensions

Parameter	ASTM D638-14 Type V	ISO 178:2003
Length (L)	82.5 ± 0.5 mm	80 ± 2 mm
Width (W)	9.5 ± 0.2 mm	10 ± 0.2 mm
Thickness (T)	~ 3.2 mm (typical)	4 ± 0.2 mm
Standard Purpose	Tensile Testing	Flexural Testing
Specimen Shape	Dog-bone	Rectangular

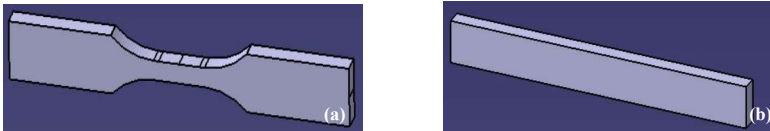


Fig.2. 3D CAD Model of (a) tensile and (b) flexural work piece

The mechanical evaluation of 3D printed CFRP and CFRP-metal sandwich structures involves standardized tensile and flexural testing procedures (Table 1). Tensile tests are conducted using specimens designed according to ASTM D638-14 Type V, which specifies the geometry and method for assessing the tensile properties of plastics. For flexural testing, the study follows the ISO 178:2003 standard, which outlines the procedure for determining flexural strength and modulus of rigid and semi-rigid plastics. These tests are essential for understanding the material's resistance to deformation under load and its overall structural integrity. The dog-bone shaped for tensile test (Fig.2(a)) and standard rectangular test pieces for flexural test (Fig.2(b)) are modelled in CAD following these standards. The tensile and flexural properties of non-sandwich CFRP specimens were analyzed first to establish a

baseline for comparison. This allows quantifying the performance gains achieved by adding metallic layers and validates the hybrid design approach. Without this baseline, improvements in stiffness, strength, and ductility cannot be accurately attributed to the sandwich configuration

3.2 3D Printing and Design of Experiments

3D printing is carried out in the Markforged 3D printer using the associated software, Eiger, enables CAD file import, G-code generation, and build parameter customization. The selected composite consists of Onyx (a nylon matrix filled with micro carbon fibers) and continuous carbon fiber reinforcement. Onyx offers high strength and stiffness, making it ideal for industrial-grade components.

Table 2. Design of experiment for selected infill patterns and infill ratio

Sl. No.	Infill pattern	Infill ratio	Tensile test ASTM D 638 (2014) type V	Flexural test ISO 178 (2003)
1	Triangular	30%	Tensile	-
2	Triangular	40%	Tensile	-
3	Triangular	52%	Tensile	-
1	Gyroid	30%	-	Flexural
2	Gyroid	40%	-	Flexural
3	Gyroid	52%	-	Flexural

Table 2 outlines the material data sheet for the plastic matrix and fiber reinforcement used in this study. In 3D printing, the infill ratio and infill pattern are key parameters that influence the internal structure and mechanical performance of printed parts. The infill ratio defines the percentage of material used to fill the interior volume of the object higher ratios enhance strength and rigidity, while lower ratios reduce weight and printing time. In Markforged 3D printers, which specialize in composite materials like CFRP), users can select from various infill patterns to tailor structural performance. This study considers two infill patterns Triangular and Gyroid- each tested at three infill ratios: 30%, 40%, and 52%. These combinations are detailed in Table 3 and are used to evaluate the influence of internal geometry on the mechanical behavior of CFRP and CFRP-metal sandwich structures.

3.3 3D Printed Specimens and Mechanical Testing

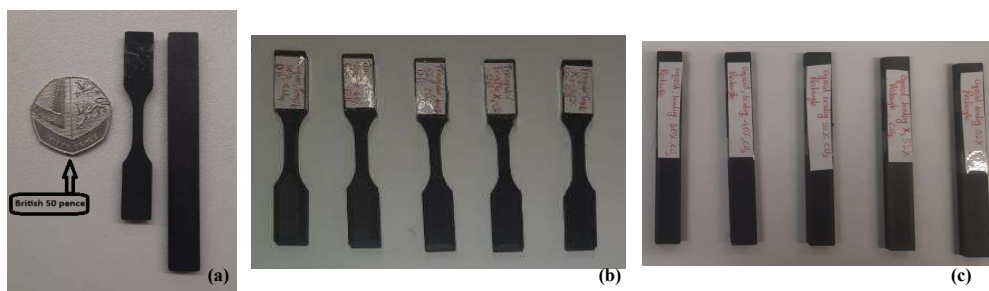


Fig.3. (a) 3D-printed specimens for tensile and flexural testing; (b) Tensile specimens with Triangular infill patterns at 30%, 40%, and 52% infill; (c) Flexural specimens with Gyroid infill patterns at 30%, 40%, and 52% infill.

Both 3D printed tensile and flexural specimens are shown in Fig. 3(a)–(c). The mechanical evaluation was carried out using the Muiset tensile testing machine (Fig. 4(a) & (b)), enabling precise measurement of properties such as elongation and tensile strength. Flexural testing was performed using an Instron Wedge Grip (Fig. 4 (c) & (d)), ensuring accurate determination of flexural modulus. These setups provide consistent and reliable assessment of the structural performance of CFRP and CFRP-metal sandwich components.

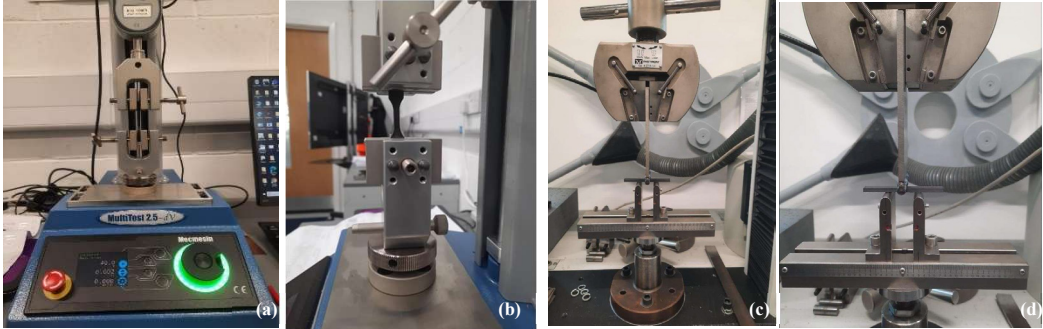


Fig.4. (a) Tensile testing setup (b) Specimen positioned between the two jaws (c) Flexural testing setup (d) Specimen positioned between the clamps

4 Analysis

4.1 Analysis of Non-Sandwich Structure - Tensile testing

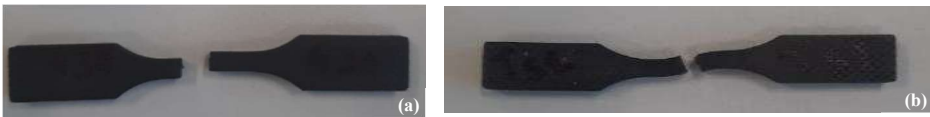


Fig. 5. (a) Gyroid infill pattern at 30% after tensile testing; (b) Triangular infill pattern at 30% before and after tensile testing.

The representative failure patterns from tensile tests are shown in Fig. 5(a) and (b). The corresponding tensile property values are presented in Table 3. From the table, a clear trend emerges: higher infill ratios result in stronger specimens for both Gyroid and Triangular infill patterns. This is expected, as increased infill density enhances structural integrity. When comparing similar infill ratios, the Triangular pattern consistently outperforms the Gyroid pattern. For example, at 30% infill, Triangular exhibits a strength of 822.1 N, slightly higher than Gyroid at 807.1 N. At 40% infill, Triangular reaches 842 N, significantly exceeding Gyroid at 521 N. Even at 52% infill, Triangular maintains superiority with 863 N compared to Gyroid’s 777.5 N. Displacement values indicate material elongation prior to failure, where lower displacement generally corresponds to stiffer configurations. Among all tested configurations, the Triangular 52% infill pattern demonstrates the highest strength, confirming its suitability for applications requiring enhanced load-bearing capacity.

Table 3. Tensile test values

Maximum load (N)	Displacement (mm)	3D printing Parameters
807.1 N	3.688 mm	Gyroid 30%
521 N	2.865 mm	Gyroid 40%
777.5 N	2.451mm	Gyroid 52%

822.100 N	3.172mm	Triangular 30%
842 N	3.729mm	Triangular 40%
863 N	3.636mm	Triangular 52%

4.2 Analysis of Non-Sandwich Structure - Flexural testing

Flexural tests were performed on the 3D-printed specimens, with representative failure patterns shown in Fig. 6(a) and (b).

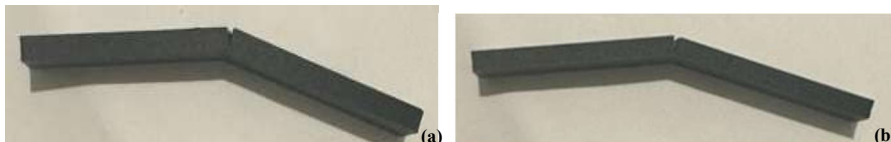


Fig.6. (a) Gyroid infill pattern at 30% density; (b) Triangular infill pattern at 40% density.

Table 4. Flexural test values

Sl. No	Infill ratio & infill pattern	Maximum loan (N)	Extension (mm)
Specimen 1	Gyroid 30%	617.433 N	2.425 mm
Specimen 2	Gyroid 40%	644.85 N	2.13 mm
Specimen 3	Gyroid 52 %	618.051 N	2.16 mm
Specimen 4	Triangular 30%	526.067 N	2.33 mm
Specimen 5	Triangular 40%	547.607 N	1.26 mm
Specimen 6	Triangular 52%	610.417 N	1.33 mm

Table 5. Specimens chosen for use in the sandwich structure

Higher strength	Lower strength
Gyroid 40% infill	Gyroid 52% infill
Triangular 52% infill	Triangular 30% infill

The corresponding flexural property values are presented in **Table 4**. Analysis of the tabulated results reveals that the Gyroid infill pattern consistently delivers higher maximum load capacities than the Triangular pattern at comparable infill ratios. For instance, Gyroid specimens withstand 617.433 N at 30% infill versus 526.067 N for Triangular, and this advantage persists at 40% infill (644.85 N vs. 547.607 N). However, increasing the Gyroid infill ratio to 52% does not yield further strength gains, with a slight decrease to 618.051 N, suggesting that higher infill ratios can introduce diminishing returns or stress concentrations. In contrast, the Triangular pattern demonstrates a steady increase in strength from 526.067 N at 30% to 610.417 N at 52%, though it never matches the peak Gyroid values. Extension data show Gyroid specimens maintain stable deformation across ratios, while Triangular infills experience reduced extension indicating increased stiffness but potentially greater brittleness at higher infill levels. Although Gyroid 30% exhibited higher tensile strength due to better bonding and stress distribution, Gyroid 40% was chosen for sandwich structures because its higher flexural load capacity (≈ 645 N) ensures superior bending resistance. The Table 5 highlights the specimens chosen for use in the sandwich structure flexural tests, based on their relative strengths. Gyroid pattern with 40% infill and Triangular pattern with 52% infill demonstrated the highest strength among the tested samples, while Gyroid with 52% infill and Triangular with 30% infill exhibited the lowest strength. Therefore, both the highest and lowest strength specimens were selected and are presented in Table 5 for comparative evaluation in the flexural testing of sandwich structures. To understand further, SEM analysis

has been performed for fractured specimens, It provides microstructural evidence supporting the mechanical performance differences between Gyroid 30% and 40% infill ratios. As shown in Fig. 7(a), the Gyroid 30% infill exhibits relatively larger voids and less dense bonding regions, which explains its higher tensile strength but limited flexural resistance. In contrast, Fig. 7(b) reveals a more compact and uniform lattice in the Gyroid 40% infill, indicating improved layer adhesion and reduced porosity. This denser topology enhances load distribution under bending, validating the selection of Gyroid 40% for sandwich structures due to its superior flexural capacity (≈ 645 N).

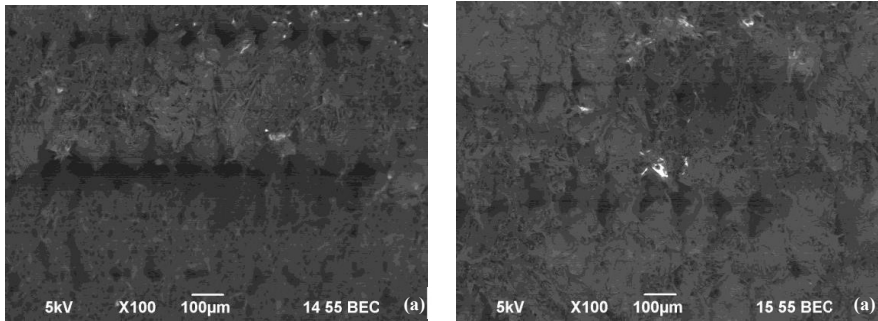


Fig.7. (a) SEM image for (a) 30% infill's gyroid topology (b) 40% Gyroid Infill

5 CFRP-Metal Sandwich Structures

5.1 Design and Optimization of CFRP-Metal Sandwich Structures

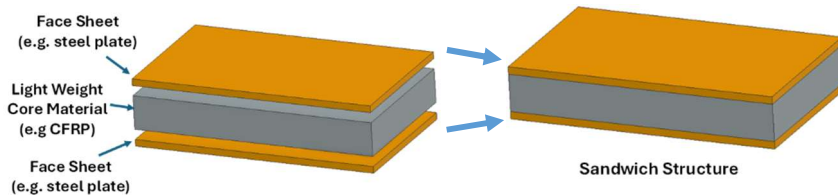


Fig.8. Simple illustration depicting the layered structure of sandwich panels

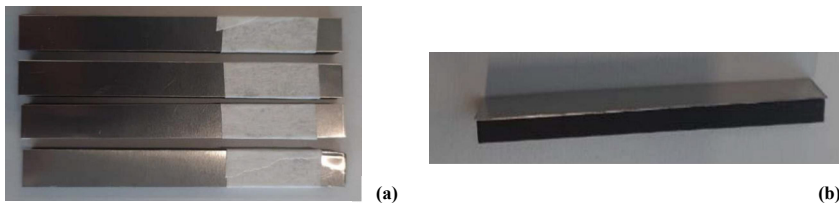


Fig.9. (a) CFRP- metal sandwiched workpieces (b) 48 CFRP - Metal sandwich workpiece side view

Based on Table 5, CFRP-metal sandwich structures / layers with infill patterns and ratios are created as a composite assembly. Fig.8 illustrates the basic layout of this sandwich structure Fig. 9 illustrate the CFRP-metal sandwich workpieces examined in this study. Fig. 9 (a) displays the overall specimens, while Fig. 9 (b) provides a side view, offering visual reference for the test configurations discussed above. Specifically, the strongest layer is composed of CFRP with a Gyroid pattern at 40% infill and a Triangular pattern at 52% infill. Conversely,

the weakest layer consists of CFRP with a Gyroid pattern at 52% infill and a Triangular pattern at 30% infill. Each CFRP layer is strategically positioned between two nickel-coated stainless-steel plates. The metallic component, made of nickel-plated stainless steel, are sandwiched and are engineered to maximize the benefits of both CFRP and metal elements. The lightweight, high-strength properties of CFRP is optimized for a balanced combination of strength, reduced weight, making it particularly suitable for applications in the aerospace and automotive industries where these qualities are essential. By carefully selecting the infill patterns and ratios within the CFRP layers, the mechanical and dynamic characteristics of the sandwich structure can be tailored to meet specific performance requirements. The assembly process involves bonding the nickel-coated stainless-steel plates to both sides of the CFRP component. The metal plates in the sandwich structure measure 80mm in length, 10mm in width, and 0.3mm in thickness. These dimensions provide a robust yet lightweight foundation for the composite assembly. Accurate sizing is essential to achieving optimal strength and conductivity in the CFRP-metal sandwich panels. Flexural tests were then performed on the 3D printed CFRP-metal sandwich specimens, with representative failure patterns shown in Fig. 10(a) and (b).

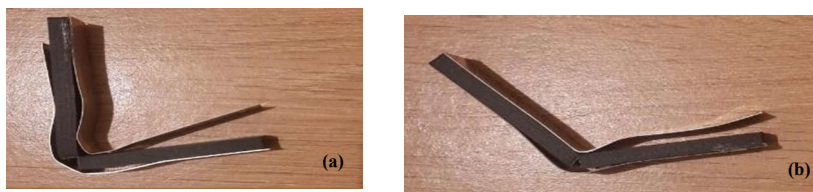


Fig. 10. Triangular pattern - Metal sandwich with (a): 30% infill ratio (b) 52% infill ratio

6 Critical Analysis of Sandwich Structure Test Results

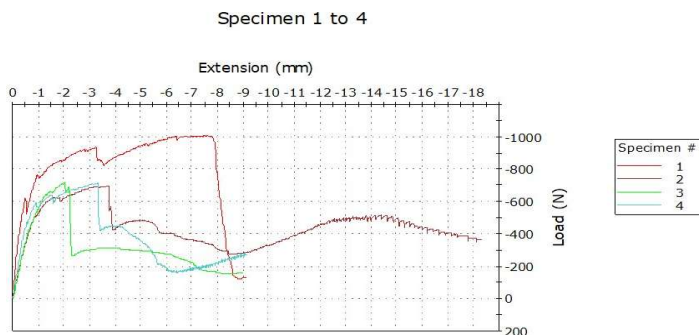


Fig. 11. Compressive Load vs. Extension for Specimens 1 to 4

Table 6. Flexural testing results for CFRP-metal sandwich specimens

Specimen	Load (N)	Extension (mm)
1. Gyroid 40% infill – Metal sandwich	1008.55 N	7.51 mm
2. Gyroid 52% infill – Metal sandwich	517.17 N	14.38 mm
3. Triangular 52% infill – Metal sandwich	717.09 N	2.03 mm
4. Triangular 30% infill – Metal sandwich	712.41 N	3.36 mm

The graph in Fig.11. presents the load-extension behavior of four specimens under compressive loading. Each curve reflects the mechanical response of a CFRP sample,

showing variation in stiffness and peak load. The data aids in evaluating consistency and structural performance across the tested configurations.

Table 6 presents mechanical testing results for CFRP-metal sandwich specimens featuring Gyroid and Triangular infill patterns at varying infill ratios. The highest load-bearing capacity is observed in the Gyroid 40% infill sandwich (1008.55 N), followed by the Triangular 52% (717.09 N) and Triangular 30% (712.41 N) infill sandwiches. Notably, the Gyroid 52% infill sandwich records a lower peak load (517.17 N) but exhibits the greatest extension (14.38 mm), indicating significant ductility compared to the other configurations. The data suggest that infill pattern and density exert a pronounced influence on the mechanical response of the sandwich structure. The Gyroid 40% infill achieves the best balance of strength and moderate extension, while increasing Gyroid infill to 52% paradoxically reduces load capacity but enhances deformation before failure. For the Triangular infill, increasing the infill ratio from 30% to 52% results in a modest increase in load capacity but a reduction in extension, implying a stiffer but less ductile structure. These outcomes highlight the complex interplay between infill geometry, density, and the interaction with the metallic face sheets in determining overall mechanical performance.

These improvements in flexural strength compared to CFRP-only specimens (Tables 3 and 4) are consistent with literature, where hybrid CFRP-metal structures have shown markedly higher load-bearing capacity than single-material laminates (Graziosi et al., 2020; Pizzorni et al., 2022). To be specific, Graziosi et al. [12] (Fig. 24, p. 14) reported peak tensile loads of approximately 20 kN for standard double-lap joints (A1), 22–23 kN for wedge-shaped interfaces (A2), and up to 27–28 kN for beam-based metal-composite junctions (A3). Similarly, Pizzorni et al. [15] (Table 6, p. 10; Fig. 14, p. 11) reported shear strengths up to 31.7 MPa (CCF/CCF) and 23.5 MPa (CFRT/CFRP). Separately, they demonstrated up to +251.4% increase in ultimate load by extending the overlap from 12.5 mm to 50 mm (Table 5, p. 6; Fig. 4). While our Gyroid 40% sandwich specimen achieved 1008.55 N in flexural loading—lower in absolute terms due to different test modes and the preliminary nature of this study it is still significant as a proof of concept. These results confirm the effectiveness of metal integration for bending resistance and provide a strong foundation for future optimization. Further improvements in interface design, material selection, and manufacturing parameters are expected to deliver performance closer to the levels reported in tensile and shear studies. Future work will focus on fatigue and impact testing under cyclic loads, optimization of bonding interfaces, and topology-driven weight reduction to advance CFRP-metal hybrid designs for hydrogen storage and aerospace applications.

6.1 Comparison with Pure Infill Tensile Tests

Comparing these sandwich structure results to tensile test data for standalone 3D-printed infill specimens reveals notable differences. Pure infill tensile tests typically show a direct correlation between increased infill ratio and enhanced tensile strength, with Gyroid and Triangular patterns demonstrating predictable trends based on their geometric characteristics. In contrast, the sandwich panels do not consistently follow this pattern; for example, the Gyroid 52% infill sandwich underperforms relative to its 40% counterpart in terms of maximum load. This divergence is attributable to the composite nature of the sandwich structure. The presence of nickel-coated stainless steel face sheets alters the stress distribution and failure mechanisms, introducing interface effects and constraining the CFRP core. The synergy between the stiff outer metal layers and the CFRP infill core can result in different failure modes—such as delamination, core shear, or face yielding—which are not present in pure tensile tests of infill specimens. The sandwich structure's behavior is thus governed by both the properties of the core and its interaction with the face sheets, rather than by the infill alone.

6.2 Discussion of Selection Rationale for Flexural Tests

The rationale for selecting specific infill patterns and ratios for sandwich flexural testing stems from the desire to optimize the balance between stiffness, strength, and weight. Gyroid and Triangular patterns were chosen due to their favorable mechanical properties and manufacturability in 3D printing. The selected infill ratios (30%, 40%, 52%) represent a range of densities to evaluate their effect on flexural performance. Lower infill ratios offer weight savings and potential energy absorption, while higher ratios aim to maximize stiffness and load-bearing capacity. The flexural test context is particularly sensitive to core shear and face-core debonding, making the sandwich configuration more representative of real-world loading scenarios than pure tensile tests.

7 Relevance to Hydrogen Storage Systems (Type I–V) and Implications for Our CFRP–Metal Sandwich Design

High-pressure gaseous hydrogen is stored today in four mature vessel classes (Type I–IV) [2-5,6] and an emerging linerless class (Type V), each defined by its liner and overwrap architecture and governed by ISO 11119/11439 [3] and vehicular performance standards such as SAE J2579 [4]. These vessel classes create different integration opportunities for our 3D-printed CFRP–metal sandwich structures. For Type I–II arrays in stations or tube-trailers, weight is a penalty; sandwich panels and brackets that use higher-stiffness/strength infills (Triangular $\geq 52\%$) can reduce balance-of-plant mass (manifold frames, saddles, crash shrouds) while maintaining rigidity under transport loads. However, when metallic facesheets or inserts operate in hydrogen environments, material selection matters: austenitic stainless steels (e.g., 316L/316LN) are widely used in hydrogen infrastructure for their better resistance to hydrogen-assisted cracking compared with metastable grades like 304/304L [20,21]; this should guide the choice of metal layers and welded fittings in our hybrid joints.

For Type III (Al liner + CFRP wrap), our results indicating greater tensile strength and stiffness with Triangular infill at higher ratios support their use in non-pressure-bearing, load-path components directly interfacing with the vessel e.g., saddle inserts, boss-ring load distributors, anti-abrasion cladding and modular mounting rails, where minimizing local deflection curbs stress concentrations in the overwrap. These subsystems must still pass SAE J2579 durability envelopes (pressure/temperature cycling, chemical and impact exposures) [4, 22, 23], which we should emulate in our later test plans for bonded sandwich assemblies.

For Type IV (polymer liner + CFRP wrap) [5,24], hydrogen permeation through the liner is a primary safety/performance constraint; HDPE (high-density polyethylene) and PA6 (polyamide 6, or nylon 6) exhibit non-zero permeation that evolves with temperature, pressure and thermal cycling [24, 25]. Our sandwich structures are not the gas barrier, but their geometric stiffness (again favoring Triangular $\geq 52\%$ infill for mounts, cradles and protective shells) can reduce liner/overwrap bending at supports and bosses, indirectly lowering strain-driven permeation and microcrack risk. When our parts enclose or contact the vessel, they must be compatible with permeation and temperature cycling regimes defined in J2579 and verified in liner studies (e.g., ORNL and recent PA6/HDPE evaluations) [26, 27]. Design rules should therefore include compliance temperatures of $-40\text{ }^{\circ}\text{C}$ to $+85\text{ }^{\circ}\text{C}$, permeation-safe clearances/vents, and adhesive systems qualified under hydrogen exposure and thermal cycling.

For Type V (linerless, all-composite), ongoing research highlights leak-tightness and manufacturing complexity as the key hurdles. While our CFRP–metal sandwiches are not intended as linerless primary vessels, our flexural findings inform ancillary structures for Type V modules (cryo-compressed guards, cradle beams, impact-absorbing outer shells)

where stiff, high-strength infills limit global deflection and help protect the pressure shell from off-axis loads and stone-chip impacts; future extensions might incorporate barrier interleaves or hybrid plies to enhance hydrogen tightness in protective skins, as explored in recent cryogenic composite studies [28,29].

7.1 Risk and material-compatibility notes that cut across all vessel types:

(i) Hydrogen embrittlement—Even though austenitic steels are preferred in piping/manifolds, susceptibility rises with cold work and strain-induced martensite (notably in 304L), so we should bias our metal layers and welded inserts toward 316L/316LN, control forming strains, and qualify welds. [20, 29]

(ii) Permeation and venting—Type IV modules require demonstrated permeation control and safe leak rates per SAE J2579; fixtures and covers we design must not trap leaked hydrogen and should include deliberate vent paths away from ignition sources. [4,21]

(iii) Qualification loads—Ancillary composite hardware mounted to tanks should be validated under pressure/temperature cycling and impact consistent with ISO 11119/J2579 protocols to avoid transferring harmful point loads to the vessel. [3, 30]

8 Conclusions and Future directions

The Triangular infill pattern at higher ratios ($\geq 52\%$) delivered the highest tensile and flexural strength in our tests, achieving 842 N in tensile loading and 717.09 N in flexural loading (Tables 3 and 6). This makes it a strong candidate for both the hydrogen storage tank body and associated mounts, frames, and structural components in Type I–IV storage modules. Similarly, the Gyroid 40% infill sandwich exhibited the best overall flexural performance with a peak load of 1008.55 N and moderate extension (7.51 mm), confirming its suitability for components requiring energy absorption and ductility. These configurations can reduce overall mass while maintaining stiffness, manage strain at tank interfaces, and comply with hydrogen safety and permeation requirements. For metallic layers, 316L-class austenitic alloys and hydrogen-qualified adhesives or welds should be prioritized, and assemblies should undergo SAE J2579-style durability testing before deployment in automotive, aerospace, or stationary hydrogen systems. Building on these results, future work will focus on fatigue and impact testing of CFRP-metal sandwich structures under cyclic and crash loads, optimization of interface bonding using advanced surface treatments or adhesive systems to minimize delamination, and topology optimization for hybrid structures to reduce weight while maintaining strength through AI-driven design tools. Additional studies will address integration with hydrogen storage systems, including liner compatibility and thermal cycling (Eun et al., [6]; Katsumata et al., [7]), and explore smart CFRP-metal hybrids incorporating sensors for structural health monitoring in high-pressure environments.

References

1. Anbalagan, A., Launchbury, E. J., Kauffman, M., Pazhani, A., & Xavier, M. A. (2023). Investigation on CFRP 3D printing build parameters and their effect on topologically optimised complex models. *Materials Today: Proceedings*.
2. Andersson, J., & Grönkvist, S. (2019). Large-scale storage of hydrogen. *International journal of hydrogen energy*, 44(23), 11901-11919.
3. International Organization for Standardization. (2020). *Gas cylinders—Design, construction and testing of refillable composite gas cylinders and tubes—Part 3: Fully wrapped fibre reinforced composite gas cylinders and tubes up to 450 l with*

- non-load-sharing metallic or non-metallic liners or without liners* (ISO 11119-3:2020). <https://www.iso.org/standard/75817.html>
4. SAE International. (2010). *SAE J2579: Technical information report for fuel systems in fuel cell and other hydrogen vehicles*. National Renewable Energy Laboratory. <https://docs.nrel.gov/docs/fy11osti/49867.pdf>
 5. Sun, W. X., Li, Y. T., Huang, W. J., Zhang, Y. M., Fan, M., Xiao, Z. M., & Li, W. G. (2026). Advances in failure assessment of Type IV hydrogen storage vessels: A critical review. *Renewable and Sustainable Energy Reviews*, 226, 116353.
 6. Eun, J. H., Ahn, H. C., & Lee, J. S. (2025). Compatibility of liner materials for type IV hydrogen storage vessels and the interlaminar properties of liner/CFRP composites. *International Journal of Hydrogen Energy*, 133, 431-439.
 7. Katsumata, S., Ogasawara, T., Uchino, T., Hirayama, N., Sakata, K., & Uzawa, K. (2025). Experimental and analytical study of a high-pressure hydrogen storage tank made of CFRP with dome-cylinder split molding structure for fuel cell vehicles. *International Journal of Hydrogen Energy*, 101, 269-279.
 8. Ubaid, J., Andrew, J. J., Cantwell, W. J., Khan, K. A., Potluri, P., & Umer, R. (2025). Performance evaluation of GNP-modified epoxy/carbon fiber composites after cryogenic thermal cycling for hydrogen storage applications. *International Journal of Hydrogen Energy*, 159, 150574.
 9. Qi, L., Gao, R., Mei, Z., Cheng, L., Min, W., Kang, D., Yu M., & Sun, Z. (2024). An investigation on enhancing the bonding properties of PA11-CFRP interface in type IV high pressure hydrogen storage vessel through nanosecond pulsed laser treatment and failure mechanism research. *International Journal of Hydrogen Energy*.
 10. Zhou, C., Lin, H., Jia, X., Yang, Z., Zhang, G., Xia, L., ... & Li, M. (2024). Impact morphology characteristics and damage evolution mechanisms in CFRP laminates for hydrogen storage cylinders. *International Journal of Hydrogen Energy*, 77, 110-125.
 11. Wang, L., Wang, B., Wei, S., Hong, Y., & Zheng, C. (2016). Prediction of long-term fatigue life of CFRP composite hydrogen storage vessel based on micromechanics of failure. *Composites Part B: Engineering*, 97, 274-281.
 12. Graziosi, S., Cannazza, F., Vedani, M., Ratti, A., Tamburrino, F., & Bordegoni, M. (2020). Design and testing of an innovative 3D-printed metal-composite junction. *Additive Manufacturing*, 36, 101311.
 13. Liu, G., Xiong, Y., & Zhou, L. (2021). Additive manufacturing of continuous fibre reinforced polymer composites: Design opportunities and novel applications. *Composites Communications*, 27, 100907.
 14. Wu, W., Xie, D., Huang, J., Wang, Q., Chen, Q., & Huang, J. (2023). Adhesion enhancement for nickel layer deposited on carbon fiber reinforced polymer (CFRP) composites by pretreatment processes for lightning strike. *The Journal of Adhesion*, 99(7), 1099-1122.
 15. Pizzorni, M., Lertora, E., & Parmiggiani, A. (2022). Adhesive bonding of 3D-printed short-and continuous-carbon-fiber composites: An experimental analysis of design methods to improve joint strength. *Composites Part B: Engineering*, 230, 109539.
 16. Lestari, W. D., Mukti, A. S., Adyono, N., Diyasa, I. G. S. M., Sari, N. K., Caesarendra, W., ... & Budiwan, I. (2025). Optimization of 3D Printing Parameters

- for Carbon Fiber Reinforced Polymer (CFRP) Material: Impact and Hardness Analysis Using Taguchi Method. *Results in Materials*, 100727.
17. Abualbandora, T. A., Alshneeqat, M. G., & Mourad, A. H. I. (2025). Impact of 3D printing parameters of short carbon fiber reinforced polymer CFRP on the mechanical and failure performance: Review and future perspective. *Next Materials*, 8, 100645.
 18. Yan, A., Deng, B., Peng, F., Yi, J., Li, Z., Shen, J., ... & Tang, X. (2025). A stepwise parameter planning methodology for 3D printing of continuous fiber reinforced polymer composites. *Composites Part A: Applied Science and Manufacturing*, 199, 109228.
 19. Bendine, K., Gibhardt, D., Fiedler, B., & Backs, A. (2022). Experimental characterization and mechanical behavior of 3D printed CFRP. *European Journal of Mechanics-A/Solids*, 94, 104587.
 20. San Marchi, C., & Somerday, B. P. (2012). Technical reference for hydrogen compatibility of materials (SAND2012-7321). Sandia National Laboratories.
 21. Somerday, B. P., & Sloane, C. S. (2019). Addressing hydrogen embrittlement of metals in the SAE J2579 fuel cell vehicle tank standard.
 22. McDougall, M. (2010). SAE J2579 validation testing program: Powertech final report (NREL/SR-5600-49867). National Renewable Energy Laboratory.
 23. Sloane, C. (2010). Test protocol for hydrogen storage systems in SAE J2579 and GTR requirements. U.S. Department of Energy.
 24. Dong, C., Liu, Y., Li, J., Bin, G., Zhou, C., Han, W., & Li, X. (2023). Hydrogen permeability of polyamide 6 used as liner material for Type IV on-board hydrogen storage cylinders. *Polymers*, 15(18), 3715.
 25. Smith, D. B. (2014). Lifecycle verification of tank liner polymers (ORNL/TM-2014/48). Oak Ridge National Laboratory.
 26. Li, X., Wang, Q., Wu, S., Wu, D., Cui, D., & Bai, J. (2025). Exploring the gas permeability of Type IV hydrogen storage cylinder liners: Research and applications. *Materials*, 18(13), 3127.
 27. Olsson, R., Cameron, C., Moreau, F., Marklund, E., Merzkirch, M., & Pettersson, J. (2024). Design, manufacture, and cryogenic testing of a linerless composite tank for liquid hydrogen. *Applied Composite Materials*, 31(4), 1131–1154.
 28. Mikroni, M., Koutsoukis, G., Vlachos, D., Kostopoulos, V., Vavouliotis, A., Trakakis, G., Athinaios, D., Nikolakea, C., & Zacharakis, D. (2024). Design, analysis, and testing of a Type V composite pressure vessel for hydrogen storage. *Polymers*, 16(24), 3576.
 29. Hughes, L. A., Somerday, B. P., Balch, D. K., & San Marchi, C. (2014). Hydrogen compatibility of austenitic stainless-steel tubing and orbital tube welds. *International journal of hydrogen energy*, 39(35), 20585-20590.
 30. International Organization for Standardization. (2002). Gas cylinders of composite construction — Specification and test methods — Part 3: Fully wrapped fibre reinforced composite gas cylinders with non-load-sharing metallic or non-metallic liners (ISO Standard No. 11119-3:2002). <https://www.iso.org/standard/28426.html>